uPAR-induced cell adhesion and migration: vitronectin provides the key

Chris D. Madsen,[1] Gian Maria Sarra Ferraris,[1] Annapaola Andolfo,[1] Orla Cunningham,[1] and Nicolai Sidenius[1,2]

[1]FIRC Institute of Molecular Oncology (IFOM), 20139 Milan, Italy
[2]Molecular Genetics Unit, DIBIT, Università Vita-Salute San Raffaele, 20132 Milan, Italy

Expression of the membrane receptor uPAR induces profound changes in cell morphology and migration, and its expression correlates with the malignant phenotype of cancers. To identify the molecular interactions essential for uPAR function in these processes, we carried out a complete functional alanine scan of uPAR in HEK293 cells. Of the 255 mutant receptors characterized, 34 failed to induce changes in cell morphology. Remarkably, the molecular defect of all of these mutants was a specific reduction in integrin-independent cell binding to vitronectin. A membrane-tethered plasminogen activator inhibitor-1, which has the same binding site in vitronectin as uPAR, replicated uPAR-induced changes. A direct uPAR–vitronectin interaction is thus both required and sufficient to initiate downstream changes in cell morphology, migration, and signal transduction. Collectively these data demonstrate a novel mechanism by which a cell adhesion molecule lacking inherent signaling capability evokes complex cellular responses by modulating the contact between the cell and the matrix without the requirement for direct lateral protein–protein interactions.

Introduction

The urokinase plasminogen activator (uPA) and its receptor (uPAR) play important roles in physiological processes such as wound healing, inflammation, and stem cell mobilization, as well as in severe pathological conditions such as HIV-1 infection, tumor invasion, and metastasis (Alfano et al., 2002; Sidenius and Blasi, 2003; Gyetko et al., 2004; Selleri et al., 2005; Lund et al., 2006). Besides uPAR's well-established role in the regulation of pericellular proteolysis, it also modulates cell adhesion, migration, and proliferation through interactions with proteins present in the extracellular matrix, including vitronectin (Vn) (Wei et al., 1994; Kjøller and Hall, 2001; Blasi and Carmeliet, 2002). The absence of transmembrane and intracellular domains renders uPAR signaling incompetent, and it is generally believed that signal transduction originating from this receptor must involve lateral interactions with transmembrane proteins. In accordance, uPAR-mediated processes have been proposed to require its interaction with membrane proteins including members of the integrin family (Wei et al., 1996), chemokine receptors (Resnati et al., 2002), and receptor tyrosine kinases (Liu et al., 2002).

Correspondence to Nicolai Sidenius: nicolai.sidenius@ifom-ieo-campus.it

Abbreviations used in this paper: GPI; glycosylphosphatidylinositol, PAI-1, plasminogen activator inhibitor-1; SMB, somatomedin-B domain; uPA, urokinase plasminogen activator; uPAR, urokinase plasminogen activator receptor; Vn, vitronectin.

The online version of this article contains supplemental material.

The important role of uPAR in tumor cell adhesion, migration, invasion, and proliferation makes this receptor an attractive drug target in cancer treatment; however, this is complicated by the extent of the published uPAR "interactome". With such a goal in mind, the most important question becomes which of the many molecular interactions are really essential to mediate uPAR function. Recently, the crystal structures of uPAR in complex with a peptide antagonist (Llinas et al., 2005) and with the N-terminal fragment of uPA (Barinka et al., 2006; Huai et al., 2006) were presented, providing the first rational basis toward understanding how uPAR may organize its multiple molecular interactions. Attempts to identify the regions in uPAR involved in the specific interaction with Vn and integrins have been published (Li et al., 2003; Degryse et al., 2005; Chaurasia et al., 2006; Wei et al., 2007); however, the results from these experiments are largely incongruent and remain to be confirmed in independent studies.

In this study we have applied a genetic approach, based on exhaustive mutagenesis and complementation experiments, to determine the essential direct molecular interactions required for uPAR to induce changes in cell morphology and migration. This was achieved in a comprehensive and unbiased way through a complete functional alanine scan of human uPAR in human embryo kidney (HEK) 293 cells. Of the 255 alanine substitutions analyzed, 34 were found to completely, or partially, impair uPAR-induced changes in cell morphology. The molecular

The Journal of Cell Biology, Vol. 177, No. 5, June 04, 2007 927–939
http://www.jcb.org/cgi/doi/10.1083/jcb.200612058

defect of all mutants was subsequently shown to be an impaired binding to the somatomedin-B (SMB) domain of Vn. Although the RGD motif in Vn was dispensable for uPAR-dependent cell binding to Vn, it was implicated in subsequent signal transduction and changes in cell morphology, underscoring the importance of integrin receptors downstream of uPAR in these processes. Although integrins are clearly involved in the cellular processes initiated by uPAR expression, we found strong evidence against any functional relevance of a direct molecular interaction between these molecules. First, all the mutants identified in the complete alanine scan have the same molecular defect (impaired Vn binding), suggesting that this is also the only required interaction. Second, alanine substitutions of the published integrin interaction sites in uPAR had no effect on receptor function. Finally, a recombinant GPI-anchored plasminogen activator inhibitor-1 (PAI-1) molecule (PAI-1/GPI), which also binds Vn, mimicked the cellular effects of uPAR expression.

We conclude that a direct Vn interaction is both necessary and sufficient to initiate uPAR-induced changes in cell morphology, migration, and signaling independently of direct lateral protein–protein interactions. The importance of the uPAR–Vn interaction was not cell type–specific, as very similar data were obtained in CHO cells.

Results

Overexpression of uPAR in 293 cells induces signal transduction and changes in cell morphology and migration

It has been previously reported that expression of uPAR modulates the adhesion and motility of 293 cells through interactions with Vn, integrins, and G protein–coupled receptors (Wei et al., 1994, 1996, 1999, 2001; Degryse et al., 2005; Gargiulo et al., 2005; Chaurasia et al., 2006;). In accordance, we find that expression of human uPAR in HEK293 Flp-In T-REx (293) cells induces changes in cell morphology, migration, and signaling (Fig. 1). The morphological changes include a general flattening of the cells, reduced cell–cell contact, disappearance of membrane ruffles, and formation of extensive lamellipodia (Fig. 1 A, left panels), as well as a complete reorganization of the matrix-proximal F-actin cytoskeleton (Fig. 1 A, right panels). The changes in cell morphology reflect the cell motility induced by uPAR expression in these cells (Fig. 1 B and Video 1, available

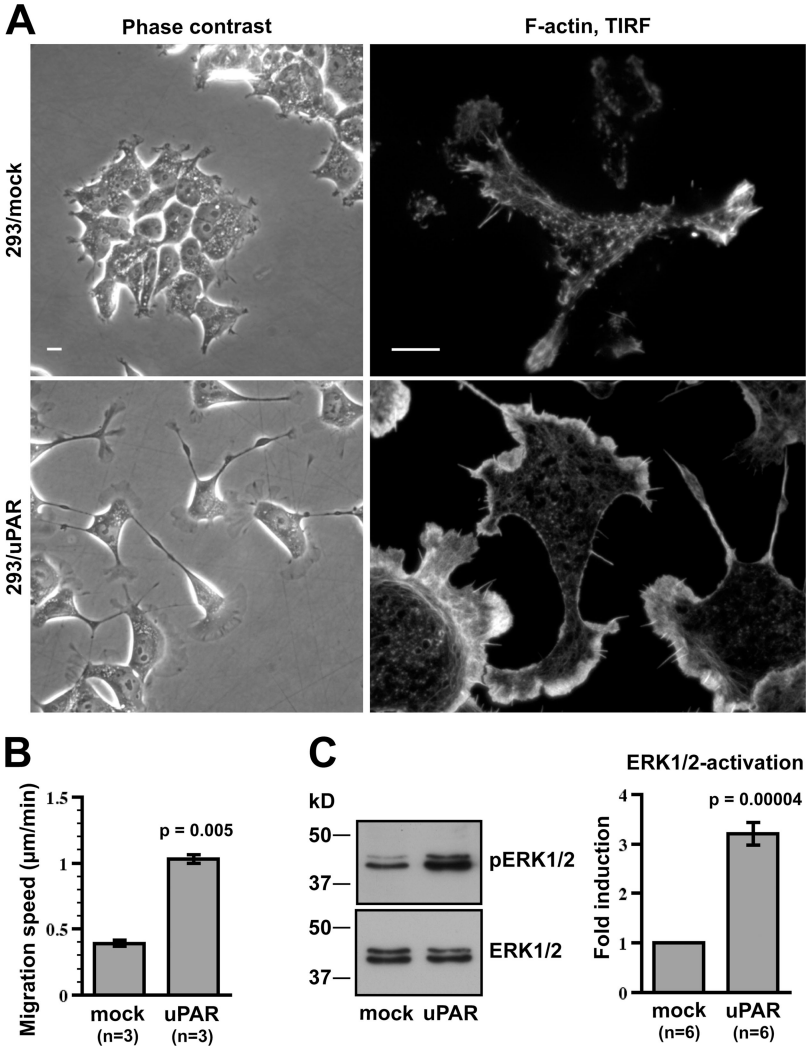

Figure 1. **Expression of uPAR in 293 cells induces changes in cell morphology, actin cytoskeleton, signal transduction, and cell migration.** (A) uPAR-induced changes in cell morphology and F-actin cytoskeleton. 293 cells transfected with a vector expressing human uPAR (293/uPAR) or empty vector (293/mock) were analyzed by phase-contrast microscopy (left panels) and by TIR-FM after fixation and staining with phalloidin-FITC (right panels). Bar, 10 μm. (B) uPAR expression induces basal cell migration. Cell migration speed was quantified using manual cell tracking of 293/mock and 293/uPAR cells monitored for 30 min (1 frame every 15 s) by phase-contrast time-lapse recordings. The entire time-lapse movie, including overlay tracking, is Video 1 (available at http://www.jcb.org/cgi/content/full/jcb.200612058/DC1). The number (*n*) of independent experiments in the dataset is indicated. The significance levels are indicated and refer to comparisons with mock-transfected cells. (C) uPAR-induced ERK1/2 activation. Semi-confluent 293/mock and 293/uPAR cells were serum starved for 4 h before cell lysis and Western blotting analysis. Blots were first probed for phosphorylated ERK1/2 (top blot) then stripped and reprobed for total ERK1/2 (bottom blot). The graph shows the mean ± SEM increase in the ratio between phosphorylated and total ERK/1/2 induced by uPAR expression. The number (*n*) of independent experiments in the dataset is indicated. The significance levels are indicated and refer to comparisons with mock-transfected cells.

at http://www.jcb.org/cgi/content/full/jcb.200612058/DC1). Migratory (Nguyen et al., 1999) and proliferative (Aguirre Ghiso et al., 1999) signaling downstream of uPAR involves activation of the Ras/MAPK signaling pathway, and in accordance we found that uPAR-expressing cells had approximately threefold increased ERK1/2 activation as compared with mock-transfected cells (Fig. 1 C).

uPAR-induced changes in cell morphology occur through Vn and require integrin-dependent RGD engagement

As previously described (Wei et al., 1994, 1996; Gargiulo et al., 2005), expression of uPAR in 293 cells resulted in a strong increase in cell adhesion to Vn, whereas adhesion to other ECM proteins including fibronectin, type-1 collagen, and laminin was unaffected (Fig. 2 A). The binding sites for uPAR and integrins on Vn are distinct, with uPAR recognizing the SMB domain (Deng et al., 1996a), and integrins the adjacent RGD motif. To address the relative importance of uPAR versus integrin binding to Vn, we performed adhesion assays using a recombinant N-terminal fragment of Vn (Vn(1–66)) that includes both the SMB domain and the RGD motif. In addition, we monitored adhesion to two variants of this fragment where either most of the SMB domain had been removed (Vn(40–66), representing essentially RGD alone), or the RGD sequence had been mutated into RAD (Vn(1–66)^{RAD}) (Fig. 2 A). Adhesion of 293/uPAR cells was supported as long as the SMB domain was present and was not affected by mutating the RGD motif. Mock-transfected 293 cells adhered poorly to all of these substrates and not at all to Vn(1–66)^{RAD} (Fig. 2 A). Profiling of Vn receptor expression by the 293 cells and antibody inhibition experiments (Fig. S1, A and B; available at http://www.jcb.org/cgi/content/full/jcb.200612058/DC1) indicated that the weak RGD-dependent adhesion of mock-transfected 293 cells to Vn was mediated by the $\alpha_v\beta_5$ integrin. Collectively, the adhesion data demonstrate that uPAR promotes cell adhesion to Vn through a direct interaction with the SMB domain, and not by inducing integrin binding to the RGD motif.

Although the RGD motif in Vn is dispensable for adhesion of 293/uPAR cells, it is at least partially required for the subsequent changes in cell morphology and signal transduction

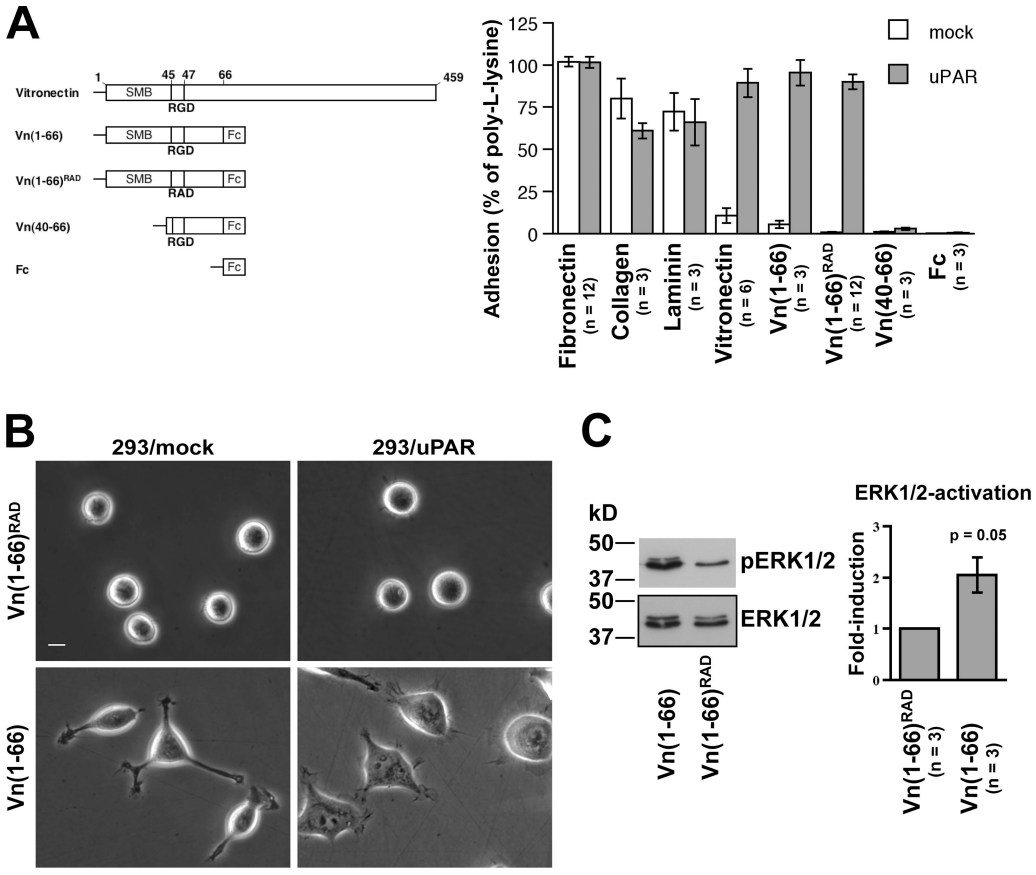

Figure 2. **uPAR induces RGD-independent cell adhesion to vitronectin and RGD-dependent changes in cell morphology and signal transduction.** (A) uPAR promotes cell adhesion to the SMB domain of Vn. Schematic representation of the recombinant Vn fragments used in this study (left). Adhesion of uPAR and mock-transfected 293 cells were assayed by allowing cells to adhere for 30 min at 37°C to plates coated with the different substrates as indicated. The adhesion is shown as the percentage of adhesion to poly-L-lysine–coated wells. Values represent the mean ± SEM of independent assays each done in quadruplicate. The number (*n*) of independent experiments is indicated. (B) RGD-dependent changes in cell morphology. Phase-contrast images of 293/mock and 293/uPAR cells seeded in serum-free medium on Vn(1–66) and Vn(1–66)^{RAD} for 2 h at 37°C. Bar, 10 μm. (C) RGD-dependent ERK1/2 activation. Serum-starved 293/uPAR cells were seeded on plates coated with Vn(1–66) or Vn(1–66)^{RAD} for 30 min. The medium was aspirated and the cell lysates prepared and analyzed by Western blotting for ERK1/2 activation as in Fig. 1. Graph indicates the mean ± SEM. The number (*n*) of independent experiments in the dataset is indicated. The significance levels are indicated and refer to comparisons with mock-transfected cells.

(Fig. 2, B and C). Although 293/uPAR cells seeded on Vn(1–66) undergo marked changes in morphology, including cell flattening and extensive lamellipodia formation, these changes are absent when seeded on $Vn(1–66)^{RAD}$, where only a round adhesion patch can be observed under the cell body. Under the same conditions, mock-transfected cells retain a rounded cell body, fail to form lamellipodia, and only extend thin membrane protrusions with limited matrix contact as evidenced also by the weak adhesive strength of these cells (Fig. 2 A). Mock-transfected cells remained completely round on $Vn(1–66)^{RAD}$ in accordance with the adhesion data. When plated on Fn, no differences in cell adhesion and morphology were observed comparing 293/mock and 293/uPAR cells (unpublished data). The level of ERK1/2 activation was higher (Fig. 2 C) when 293/uPAR cells were seeded on Vn(1–66) as compared with $Vn(1–66)^{RAD}$, suggesting that also uPAR-induced downstream signaling is at least partially integrin dependent.

In summary, these data show that the ability of uPAR to induce changes in 293 cell morphology is a two-step process in which uPAR, through the direct interaction with the SMB domain of Vn, triggers cell attachment to the matrix. Subsequently, this initial adhesion is followed by engagement of integrins, possibly $\alpha_v\beta_5$, with matrix Vn, triggering changes in cell morphology, migration, and signal transduction.

A direct Vn interaction is fundamental for the ability of uPAR to induce changes in cell morphology

In addition to the direct interaction with matrix Vn, extensive data suggests that the ability of uPAR to modulate cell adhesion, migration, and proliferation requires a complex network of lateral interactions with a variety of membrane proteins including integrins, receptor tyrosine kinases, and chemokine receptors. To address the nature of these lateral uPAR interactions in a comprehensive and unbiased fashion, we next conducted a complete functional alanine scan of uPAR in 293 cells. Receptor-induced changes in 293 Flp-In T-REx cells were chosen for this purpose for two reasons: (1) as shown in Fig. 1, uPAR expression in these cells causes very evident changes in cell morphology which can be scored easily by phase-contrast microscopy; and (2) in addition, the Flp-In system generates pools of isogenic transfectants carrying a single copy of the expression cassette, thus eliminating potential artifacts caused by clonal differences or heterogeneous expression levels.

We generated 255 single amino acid substitution mutants of uPAR by site-directed mutagenesis (all residues of mature uPAR excluding 28 cysteines) and expressed these in 293 Flp-In T-REx cells. As expected, the cell surface expression of all mutant receptors was similar and comparable to that of wild-type uPAR as evaluated by FACS analysis and immunoblotting (Table I; Fig. S1, C and D; and Table S1 for a complete listing).

Of the 255 receptor variants analyzed, 34 were found to fully or partially impair the ability of uPAR to induce changes in cell morphology (listed in Table I). None of these residues coincided with previously identified interaction sites for Vn or integrins (Li et al., 2003; Degryse et al., 2005; Chaurasia et al., 2006; Wei et al., 2007), but several are known to be involved in uPA binding (Gardsvoll et al., 2006). As the 293 cells do not express uPA (Wei et al., 1994), the molecular defect of these mutants could not be explained by available evidence. Five of the mutants were found to suffer from severe folding problems as evidenced by the presence of high molecular weight covalent aggregates in immunoblotting experiments, and were not analyzed further (Table I and Fig. S1 D).

Because the initial step in uPAR-induced signaling and cell morphology changes is triggered by the direct binding to the SMB domain of Vn (Fig. 2), we next analyzed the adhesive properties of cells expressing the remaining 29 mutant receptors with impaired ability to change cell morphology (Fig. 3). Remarkably, all of the mutant receptors displayed an impaired ability to promote cell binding to $Vn(1–66)^{RAD}$ (Fig. 3 A). There was a strong correlation between the ability to induce changes in cell morphology and the reduction in uPAR binding to the SMB domain of Vn (Fig. 3 B), demonstrating a direct link between these parameters. Receptor mutants that did not impair the ability of uPAR to induce changes in cell morphology (S56A) as well as receptors containing mutations in published integrin interaction sites (E134A/E135A, S245A, H249A, and D262A) all displayed normal adhesion to the same substrate. All cell lines adhered equally well to Fn (Fig. S2 A, available at http://www.jcb.org/cgi/content/full/jcb.200612058/DC1). Ligand binding has been demonstrated to enhance uPAR-dependent cell adhesion to Vn, and we therefore also performed the adhesion experiments in the presence of exogenously added pro-uPA (Fig. 3 C). Under these conditions the adhesion of most of the mutants was restored to that of wild-type uPAR, suggesting that ligand binding may compensate for the molecular defect of most of these mutants. The rescued Vn adhesion was also associated with restored uPAR cell morphology when cells were cultured in the presence of pro-uPA (Fig. S2 B). For some mutants (in particular W32A and R91A) cell adhesion and uPAR morphology was only partially recovered by the addition of pro-uPA, suggesting that these may be key residues for the uPAR–Vn interaction.

Identification of the Vn interaction site in uPAR

The location of the mutated residues on the published crystal structure of uPAR combined with the relatively small size of the SMB domain suggest that only part of the identified residues actually engage SMB directly. To identify this subset we next generated and expressed soluble variants of the mutant receptors and assessed their binding to immobilized Vn (Sidenius et al., 2002). As we were seeking residues in the direct molecular interaction interface, the analysis was restricted to the 19 mutant receptors where the substituted amino acid exhibits a surface exposure area on the published crystal structure above $15Å^2$. In these binding assays, five mutants (W32A, R58A, I63A, R91A, and Y92A) were found to display greater than fivefold reduction in binding to immobilized Vn (Fig. 3 D) while still having a normal binding to immobilized pro-uPA (unpublished data), suggesting that these residues are involved in the direct interaction with Vn. The impaired Vn binding of these mutants was observed also in the presence of excess pro-uPA, suggesting (Sidenius et al., 2002) that the defect of these

mutants is not related to impaired uPAR dimerization (unpublished data).

On a molecular surface representation of the uPAR structure (Fig. 3 E), W32 and R91 define a composite epitope with residues located in both domain 1 and 2 of uPAR. The residues affected by the R58A, I63A, and Y92A substitutions are all located close to these residues, suggesting that they may also engage Vn directly. The Vn-binding epitope is located distal to the membrane anchorage position (indicated in cyan) and lies on the "top-back" of the molecule with respect to the central uPA-binding cavity. Although we currently do not know the precise molecular explanation for the failure of the remaining mutant receptors to bind to Vn in the absence of pro-uPA, it should be stressed that from a functional point of view their defect is identical to that of W32A and R91A, i.e., impaired Vn binding.

The binding to matrix Vn is the only direct uPAR interaction required to trigger changes in cell morphology, migration, and signaling

The fact that all the mutants with impaired ability to induce changes in cell morphology share the same molecular defect in RGD-independent Vn binding suggests that this may also be the only important uPAR interaction required to trigger changes in cell morphology, migration, and signaling. This is particularly intriguing because the ability of uPAR to modulate cell adhesion and migration has been shown previously to require direct uPAR–integrin interactions (Wei et al., 1996, 2007; Degryse et al., 2005; Gargiulo et al., 2005; Chaurasia et al., 2006). Individual (not depicted) or combined alanine substitutions (E134A/E135A/S245A/H249A/D262A, termed uPAR/Int$^-$) in the published integrin binding sites in uPAR had no effect on the ability

Table I. **Alanine substitutions in uPAR, which impair uPAR-induced morphology changes in 293 cells**

Mutant	293 Morph.[a]	FACS[b] (mean ± SD)	Folding[c]	Surface exp.[d] (Å^2)
L1A	intermediate	116 ± 40	misfolded	45
T26A	intermediate	168 ± 4	normal	2
L31A	mock	81 ± 18	normal	32
W32A	mock	97 ± 9	normal	69
E39A	intermediate	95 ± 5	normal	99
K43A	mock	89 ± 9	normal	24
N52A	mock	112 ± 4	normal	71
R53A	mock	122 ± 9	normal	46
T54A	mock	118 ± 13	normal	19
L55A	mock	158 ± 33	normal	38
Y57A	mock	100 ± 4	normal	51
R58A	mock	90 ± 6	normal	67
G60A	mock	100 ± 4	normal	54
I63A	mock	131 ± 14	normal	32
T64A	intermediate	108 ± 8	normal	17
L66A	intermediate	96 ± 7	normal	61
E68A	intermediate	101 ± 9	normal	33
V70A	mock	104 ± 34	normal	33
L75A	intermediate	108 ± 5	normal	51
N77A	mock	82 ± 38	misfolded	0
R91A	mock	66 ± 12	normal	
Y92A	mock	61 ± 6	normal	99
L93A	mock	121 ± 1	misfolded	39
S97A	intermediate	86 ± 6	normal	0
L113A	mock	98 ± 17	normal	14
E120A	mock	134 ± 27	normal	12
L123A	mock	112 ± 40	normal	5
R145A	intermediate	159 ± 57	normal	0
G146A	intermediate	80 ± 25	normal	0
F159A	mock	277 ± 5	misfolded	1
F165A	mock	182 ± 63	normal	0
F167A	intermediate	103 ± 36	normal	14
N177A	mock	145 ± 74	misfolded	4
G179A	intermediate	101 ± 8	normal	31

[a]The cell morphology of transfected 293 cells (morph.) is divided into three groups; wild-type uPAR morphology (uPAR), mock transfected morphology (mock), and intermediate morphology (intermediate).
[b]Cell surface receptor expression was measured by FACS analysis. The mean fluorescence (± SD) represents an average of three independent antibodies correlated to the expression level of wild-type uPAR.
[c]The overall protein folding of the receptors was monitored by non-reducing SDS-PAGE and immunoblotting.
[d]Surface exposure area (Å^2) of the individual residues on the crystal structure of uPAR (PDB entry 1YWH) is indicated. No surface exposure is indicated for R91, as this residue is not defined in the crystal structure. A complete list of all mutants analyzed can be found in Table S1.

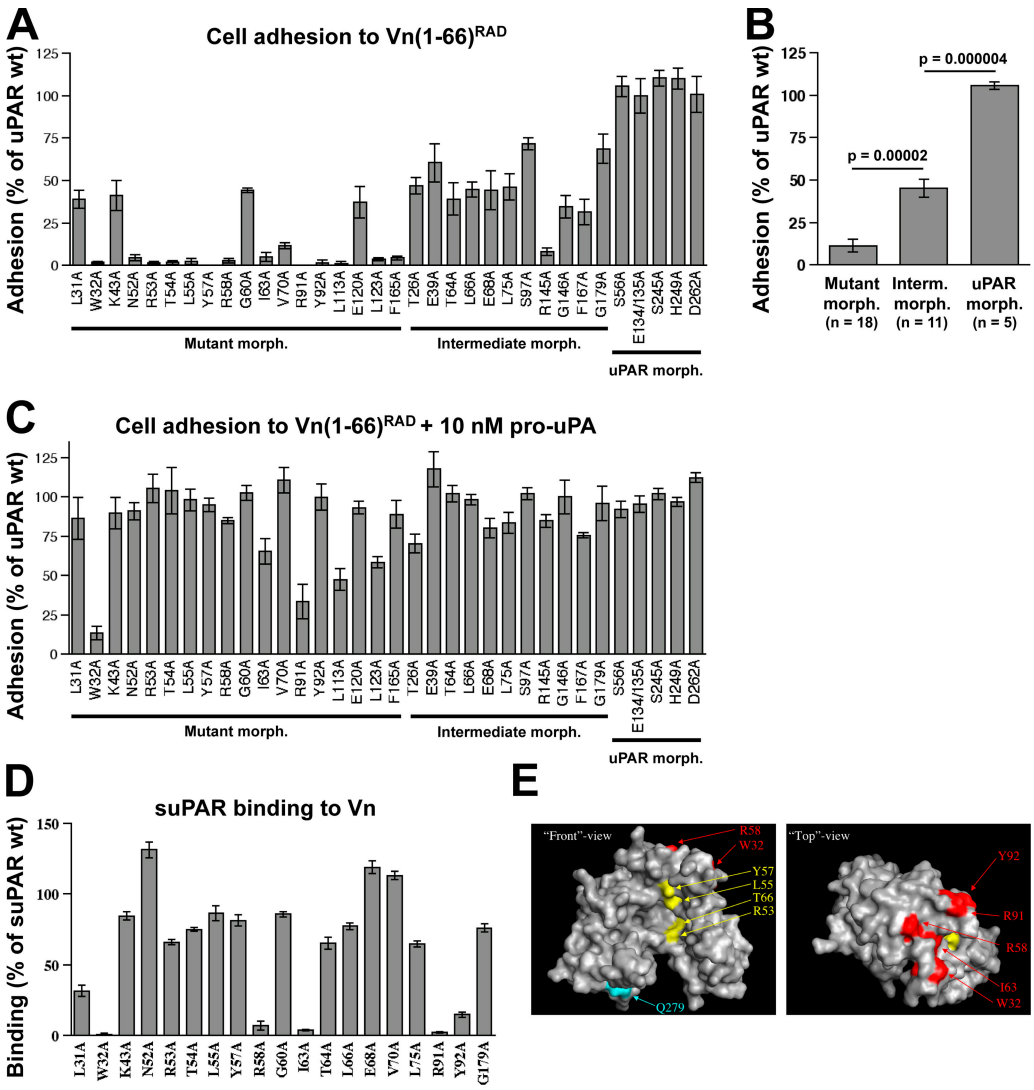

Figure 3. **The ability of uPAR to induce changes in cell morphology requires a direct Vn interaction.** (A) Adhesion to Vn(1–66)^{RAD} of cells expressing uPAR single alanine substitution mutants, which completely (Mutant morph.) or partially (Intermediate morph.) fail to induce changes in 293 cell morphology. Four mutants that induced normal uPAR-like changes in cell morphology (uPAR morph.) were included in the analysis for comparison. The data are presented as the mean ± SEM of three independent experiments, each performed in quadruplicate as described in Fig. 1. (B) Correlation between cell morphology and cell adhesion to Vn(1–66)^{RAD}. Summary of the level of cell adhesion to Vn(1–66)^{RAD} as grouped by the mutants ability to induce morphology changes. The number (*n*) of uPAR mutants in each morphological group is indicated. Data are presented as means ± SEM. (C) Adhesion to Vn(1–66)^{RAD} as shown in panel A but with the adhesion conducted in the presence of 10 nM pro-uPA. (D) Identification of the direct Vn-binding epitope using purified proteins. Soluble uPAR variants of the mutant receptors were tested for their ability to bind immobilized Vn. The mutants are arranged according to the position in the uPAR sequence. The data are presented as the mean ± SEM of three independent experiments each performed in triplicate. (E) Location of the Vn-binding site on the crystal structure of uPAR. A surface representation of the uPAR structure is shown in gray, and the positions of the alanine-substituted residues that cause a strong reduction in Vn binding using purified proteins are indicated in red. For comparison, a series of residues located in the uPAR ligand binding cavity and known to be involved in uPA binding are indicated in yellow. The most C-terminal residue (Q279) that is likely to be located close to the GPI anchor of membrane-tethered uPAR is indicated in cyan. The left panel is a "front" view of the uPA-binding cavity (Llinas et al., 2005) and the right panel is a "top" view (front view rotated 90° toward the observer). The images were constructed using the coordinates deposited in the Protein Data Bank (PDB) with the code number 1YWH and the MacPyMOL software (http://pymol.sourceforge.net).

of uPAR to induce changes in cell morphology and F-actin cytoskeleton (Fig. 4 A), Vn-adhesion (Fig. 4 B), signaling (Fig. 4 C), and cell migration (Fig. S3 A, available at http://www.jcb.org/cgi/content/full/jcb.200612058/DC1). On the other hand, a single alanine substitution in the Vn-binding epitope (W32A) completely abolished all these cellular effects of uPAR expression. Although these data argue strongly against any functional relevance of direct integrin interaction(s) for the biological activity of uPAR in our cell system, the single amino acid substitution strategy does not allow us to exclude the existence of additional and functionally redundant binding sites for integrins in uPAR.

To directly address the possibility that no lateral interactions are required for the observed biological effects of uPAR expression, we conducted a genetic complementation experiment. PAI-1 shares no sequence or structural homology with uPAR; however, both molecules bind the SMB domain of Vn (Deng et al., 1996a). The Vn-binding site in PAI-1 is located distal from

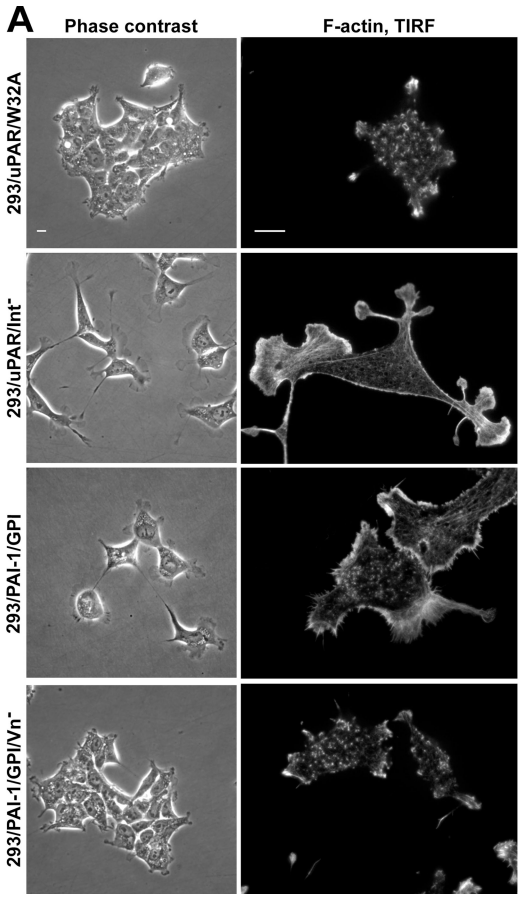

Figure 4. **A GPI-anchored PAI-1 chimeric molecule mimics uPAR function.** (A) Analysis of cell morphology (left panels) and F-actin cytoskeleton (right panels) of 293 cells expressing uPAR mutants with deficient Vn binding (W32A), integrin interaction deficient (Int^-) or the GPI-anchored PAI-1 molecule (PAI-1/GPI), and PAI-1/GPI molecule deficient in Vn binding (PAI-1/GPI/Vn^-) were analyzed as described in Fig. 1. Bar, 10 μm. (B) Adhesive properties of 293 cells expressing uPAR/W32A, uPAR/Int^-, PAI-1/GPI, and PAI-1/GPI/Vn^-. Data are presented as the mean ± SEM of three independent experiments performed in quadruplicate as described in Fig. 1. (C) ERK1/2-activation of 293 cells expressing uPAR/W32A, uPAR/Int^-, PAI-1/GPI, and PAI-1/GPI/Vn^-. Serum-starved cells were analyzed for ERK1/2 activation as described in Fig. 1. A representative immunoblot is shown and the quantification of (*n*) independent experiments is graphed as the mean ± SEM. Significance levels are indicated and refer to comparisons with mock-transfected cells analyzed in parallel.

the C terminus to which we attached the GPI-anchoring signal of uPAR (Fig. S3 B). The resulting membrane-tethered PAI-1 (termed PAI-1/GPI) was efficiently expressed on the cell surface (Fig. S3 C) and induced strong cell binding to $Vn(1–66)^{RAD}$ (Fig. 4 B). Remarkably, the expression of PAI-1/GPI in 293 cells induced changes in cell morphology, adhesion, and ERK1/2 activation comparable to those induced by uPAR (Fig. 4, A–C). The ability of PAI-1/GPI to induce these changes in cell morphology strictly required its interaction with Vn, as the introduction of a triple alanine substitution that efficiently disrupts its interaction with Vn (R103A/M112A/Q125A, termed PAI-1/GPI/Vn^-) (Jensen et al., 2004) failed to induce any of these changes (Fig. 4, A–C).

Together these data demonstrate that a direct uPAR–Vn interaction is both required and sufficient to trigger changes in cell morphology, migration, and signal transduction. Other crucial molecular events downstream of this interaction, including integrin engagement of the RGD motif in Vn, do not require any additional direct uPAR interactions.

A direct Vn interaction is required and sufficient for uPAR to induce changes in cell morphology, adhesion, and signaling in CHO cells

The central importance of the Vn interaction in the biology of uPAR is not cell type specific. When seeded at low density, CHO cells form colonies with an epithelial-like morphology characterized by tight cell–cell contact and a highly defined colony contour (Fig. 5 A, left panels). In sharp contrast, CHO cells expressing high levels of uPAR form sparse colonies with no cell–cell contact. The expression of uPAR is also associated with marked changes in the organization of matrix-proximal F-actin cytoskeleton (Fig. 5 A, right panels). In analogy to the 293 cell line, uPAR expression was associated with a strong and specific increase in RGD-independent cell adhesion to Vn (Fig. 5 B) and caused increased ERK1/2 activation (Fig. 5 C).

Despite the obvious differences between the morphological features of CHO and 293 cells, the direct Vn interaction was found to be required for the cellular effects of uPAR also in this cell line (Fig. 5). Alanine substitution in the Vn binding site (W32A) abolished the ability of uPAR to induce scattering of cells, changes in F-actin cytoskeleton, and ERK1/2 activation. As observed with the 293 cells, the exogenous addition of pro-uPA rescued the uPAR cell morphology in a mutant-dependent manner (Fig. S4, available at http://www.jcb.org/cgi/content/full/jcb.200612058/DC1). Furthermore, single alanine substitutions (not depicted) or combinations of substitutions in the published integrin interaction sites had no effect on uPAR function. Finally, the PAI-1/GPI receptor replicated uPAR-induced changes in a Vn-dependent manner also in this cell line.

A direct uPAR–Vn interaction is required for uPA-induced cell changes

All the mutants identified in this study fail completely or partially to induce cell adhesion to Vn in the absence of pro-uPA (Fig. 3 A),

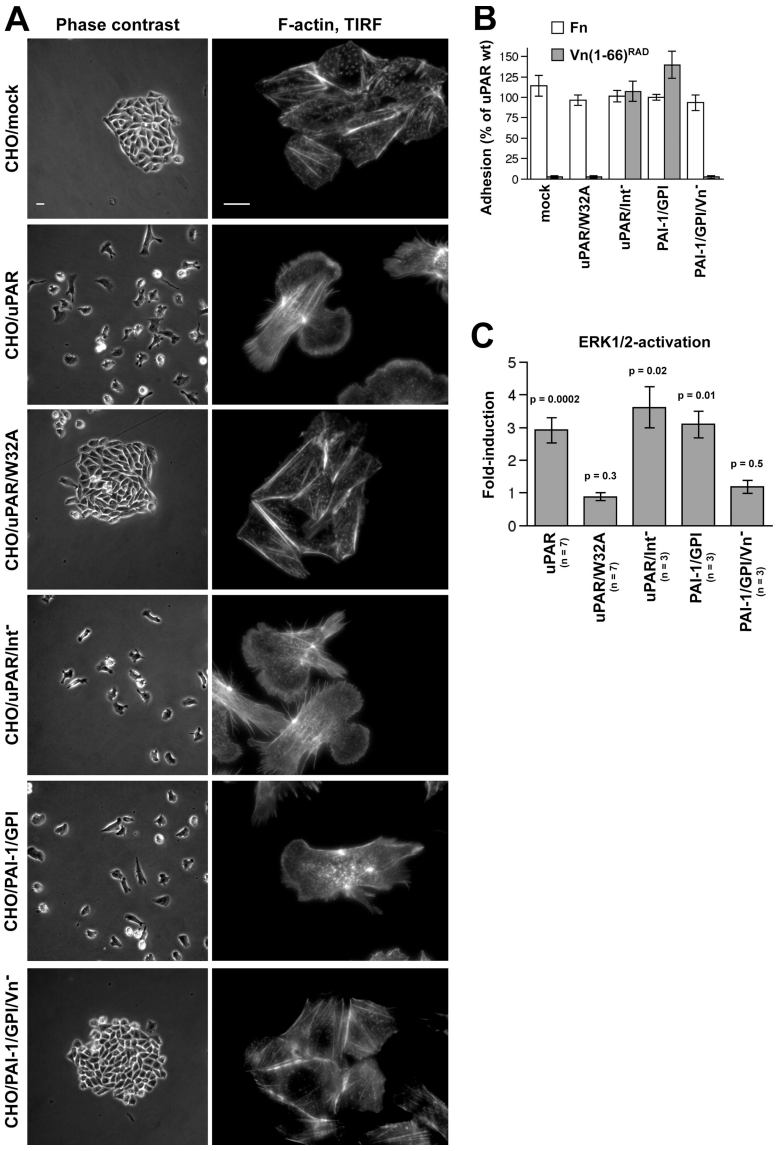

Figure 5. **A direct uPAR–Vn interaction is required and sufficient to induce changes in cell morphology, actin cytoskeleton, and signaling of CHO cells.** (A) Cell morphology (left panels) and F-actin cytoskeleton (right panels) of CHO cells transfected with empty vector (mock), wild-type uPAR, the indicated uPAR mutants, and PAI-1/GPI constructs were analyzed as described in Fig. 1. Bar, 10 μm. (B) Adhesive properties of CHO cells transfected as in A. Data are shown as the mean ± SEM of three independent assays each done in quadruplicate as described in Fig. 2. (C) ERK1/2 activation in CHO cells. Cells were serum starved overnight and analyzed for ERK1/2 activation as described in Fig. 1. The graph indicates the mean ± SEM of (*n*) independent experiments. The significance levels are indicated and refer to comparisons with mock-transfected cells.

yet their adhesive properties are in most cases restored to normal levels in the presence of exogenous pro-uPA (Fig. 3 C). As most of these mutants bind pro-uPA normally (unpublished data), they provide an important tool to dissect the importance of the direct Vn interaction in signal transduction induced by uPA binding as well as for the analysis of the cellular processes occurring subsequent to Vn engagement of the receptor. In the absence of exogenous pro-uPA expression of W32A and T54A mutant receptors both fail to induce cell binding to Vn (Fig. 6 A) and both display a low level of ERK1/2 activation similar to that of mock-transfected cells (Fig. 6 B). In the presence of the pro-uPA, cells expressing the T54A receptor, but not the W32A receptor, display a fully restored Vn binding (Fig. 6 A) and ERK1/2 activation state (Fig. 6 B). For comparison the Vn binding and ERK1/2 activation is constitutively high in cells expressing wild-type uPAR and only moderately affected by the addition of uPA. As the wild-type, W32A and T54A receptors all bind pro-uPA equally well these data document that uPA signaling to ERK1/2 occurs through the induction of uPAR binding to Vn.

The recovery of Vn binding and ERK1/2 activation induced by pro-uPA on cells expressing uPAR/T54A is paralleled by rapid changes in cell morphology and focal contact turnover as illustrated by the translocation of paxillin-GFP into newly formed lamellipodia (Fig. 6 C and Video 2, available at http://www.jcb.org/cgi/content/full/jcb.200612058/DC1) and by the scattering of preformed CHO colonies (Fig. 6 D and Video 3), which resembles a bona fide epithelial–mesenchymal transition. None of these uPA-induced changes were observed in cells expressing uPAR/W32A, underscoring the fundamental requirement for a direct uPAR–Vn interaction in these cellular processes.

Discussion

Using a systematic and unbiased approach, we demonstrate that a direct interaction between cell surface uPAR and the extracellular protein Vn is required for the ability of uPAR to modulate changes in cell morphology, migration, and signal transduction

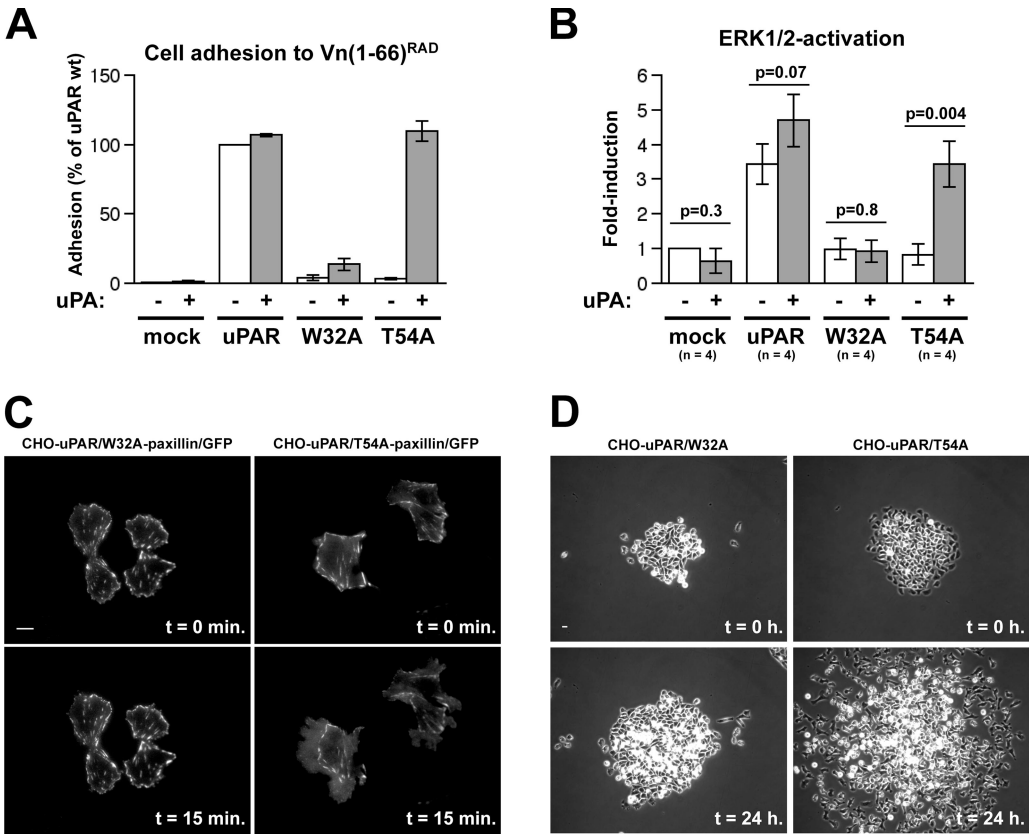

Figure 6. **A direct uPAR–Vn interaction is responsible for uPA-induced ERK1/2 activation, lamellipodia formation, and cell scattering.** (A) Adhesion to Vn(1–66)^{RAD} of CHO cells transfected as indicated were assayed in the absence or presence of 10 nM pro-uPA. Data are shown as the mean ± SEM of three independent assays each done in quadruplicate. (B) ERK1/2-activation by uPA. CHO cells transfected as above were serum starved overnight and incubated for 10 min with 10 nM pro-uPA or left untreated. After cell lysis the levels of ERK1/2 activation was quantified as described in Fig. 1. Data are shown as the mean ± SEM of (*n*) independent experiments. The significance levels are indicated and refer to comparisons between with and without pro-uPA treatment. (C) Turnover of focal contacts induced by Vn engagement of uPAR. CHO cells expressing uPAR mutants W32A and T54A were transfected with a construct encoding GFP-tagged paxillin to label focal contact. Time-lapse recordings of paxillin distribution by TIR-FM were started immediately after the addition of 10 nM pro-uPA and continued for 15 min at 4 frames/min. The panel shows the first (t = 0 min) and last (t = 15 min) frames of representative recordings. The entire movie is Video 2 (available at http://www.jcb.org/cgi/content/full/jcb.200612058/DC1). (D) Epithelial–mesenchymal transition-like scattering of CHO cell colonies induced by Vn engagement of uPAR. CHO cells expressing the W32A and T54A receptors were plated at low density and allowed to form colonies for 4 d. Phase-contrast time-lapse recordings were started immediately after addition of 10 nM pro-uPA and continued for 24 h (1 frame every 5 min). The panel shows the first (t = 0 h) and the last (t = 24 h) frames of representative recordings. The entire time-lapse movie is Video 3 (available at http://www.jcb.org/cgi/content/full/jcb.200612058/DC1). Bars, 10 μm.

in two different cell lines. This conclusion is based on two central observations. All of the alanine substitutions that affect the ability of uPAR to induce changes in cell morphology and migration directly affect uPAR-mediated cell binding to Vn independently of integrin binding to the RGD motif of Vn. Furthermore, a GPI-anchored PAI-1 molecule, which shares only the binding site in the SMB domain of Vn with uPAR, induces cellular changes that are virtually identical to those induced by uPAR.

It has been extensively documented that the ability of uPAR to modulate cell adhesion, migration, and proliferation occurs through the regulation of integrin signaling (Wei et al., 1996; Degryse et al., 2005; Gargiulo et al., 2005; Chaurasia et al., 2006). Our data are fully in accordance with this view as we observe that the RGD motif in Vn is involved in uPAR-mediated downstream signal transduction and changes in cell morphology. Nevertheless, our data argue firmly against a functionally relevant direct interaction between uPAR and integrins. Alanine substitutions in the previously published integrin interaction sites, alone or in combination, have no effect on uPAR function in both cell lines analyzed. We found no mutants with normal RGD-independent Vn binding and impaired ability to induce changes in cell morphology. Finally, an engineered PAI-1/GPI molecule, which recapitulated the membrane–ECM interaction induced by uPAR, was sufficient to induce similar changes. Our data do not rule out direct uPAR–integrin interactions; however, they do allow us to conclude that if these interactions occur they are of little or no functional importance with respect to uPAR-induced changes in cell morphology, migration, and signaling, at least in 293 and CHO cells.

Based on binding assays using purified proteins and the presence of pro-uPA, we were able to identify five residues (W32, R58, I63, R91, and Y92) that, when mutated into alanine, impair the ability of uPAR to interact with Vn. Noticeably, when these five mutants were tested for their ability to mediate cell attachment to Vn in the presence of uPA, only two of them

(W32 and R91) were still significantly impaired. These two residues are therefore likely to represent the most important direct interaction site for Vn in uPAR. That we have identified the bona fide Vn-binding epitope in uPAR is supported by several structural, functional, and evolutionary observations: the binding epitope is located distal to the GPI anchor, as would be expected for a membrane receptor that interacts with a component of the ECM. The location of the binding site is different from the location of the uPA-binding site, allowing for the simultaneous binding of these two molecules. The composite epitope contains residues both in domain 1 (W32, R58, and I63) and domain 2 (R91 and Y92), explaining why proteolytic cleavage between these two domains abolishes binding (Høyer-Hansen et al., 1997; Sidenius and Blasi, 2000). All the residues in the identified epitope are exposed on the crystal structure of uPAR. Finally, all the residues are highly conserved between different species.

How do we explain the mutants with impaired cell binding to Vn but normal binding when purified proteins are used? In contrast to cell binding assays, the binding of soluble uPAR to immobilized Vn cannot be measured in the absence of uPA (Sidenius et al., 2002). Several of the mutants (R53, L55, Y57, L113, E120, L123, R145, and G146) are located in the area of contact between domain 1 and 2 of uPAR, suggesting that the correct "docking" of these two domains is critical for Vn binding. Binding of uPA, which engages extensive areas of both domain 1 and 2 of uPAR (Gardsvoll et al., 2006; Huai et al., 2006), may compensate for this defect by enforcing the correct Vn binding competent alignment of these two domains. In addition, the N52 and T54 mutants suggest that in the absence of uPA, glycosylation of uPAR at N52 is required for Vn binding. Particularly intriguing is the finding that several of the mutant residues (L31, R53, L55, Y57, T64, L66, and E68) have their side chains exposed inside the uPA-binding cavity of uPAR. The fact that these residues were identified in a screen where uPA is absent suggests that something else, which is required for the ability of uPAR to bind Vn, is engaging this cavity in the absence of uPA and that this engagement is required for uPAR binding to Vn. The identity of this interaction has yet to be established, but based on the finding that uPAR binding to Vn involves receptor dimerization (Sidenius et al., 2002; Cunningham et al., 2003), it is tempting to speculate that this interaction partner may be uPAR itself.

Interestingly, part of the Vn binding site identified in this study (R91 and Y92) maps to the previously identified chemotactic epitope SRSRY located in the linker region connecting domain 1 and 2 of uPAR (Fazioli et al., 1997). However, it seems unlikely that this chemotactic activity is important in our cell systems, as most of the critical residues identified in this study do not map to this region, yet they do share the same molecular defect. Furthermore, PAI-1 does not contain an SRSRY sequence, yet does it mimic uPAR function. Interestingly, peptides covering this region (uPAR aa 84–95) have been shown to inhibit uPAR-dependent cell adhesion to Vn (Liang et al., 2003).

Although PAI-1/GPI closely mimic uPAR function with respect to the changes in cell adhesion, morphology, and signal transduction presented in this work, this molecule should be used as a uPAR mimic with caution, as it has cellular effects which are not seen with uPAR. These effects include a pronounced tendency of the CHO cells to "lose pieces", possibly because of an impaired lamellipodia retraction, as well as an impaired cytokinesis in the 293 cells (unpublished data). These effects are likely due to the fact that PAI-1 binds with much higher affinity to Vn than uPAR (Okumura et al., 2002).

In line with several other studies (Jo et al., 2003; Gargiulo et al., 2005; Chaurasia et al., 2006; Mazzieri et al., 2006), we observe that overexpression of uPAR leads to increased ERK1/2 activation in both cell lines analyzed. A direct uPAR–Vn interaction is required for this activation, as Vn binding–deficient uPAR mutants display levels of active ERK1/2 comparable to those of mock-transfected cells. Interestingly, uPA binding to uPAR also leads to ERK1/2 activation in different experimental systems (Nguyen et al., 1998; Aguirre Ghiso et al., 1999), suggesting that both overexpression of the receptor and ligand binding induces the same signal transduction pathway(s), possibly through a common molecular mechanism. In line with other studies we have used systems with high-level expression of uPAR ($\sim 3 \times 10^6$ binding sites per cell in both cell lines as determined by binding assays using Eu^{3+}-labeled pro-uPA; unpublished data), and under these conditions cell adhesion to Vn is independent of pro-uPA binding to uPAR (Wei et al., 1994, 1996; Cunningham et al., 2003). At physiological expression levels, uPAR-dependent cell adhesion to Vn requires uPA binding (Waltz and Chapman, 1994; Sidenius and Blasi, 2000; Sidenius et al., 2002). Consequently, it appears likely that uPA binding may actually induce "Vn signaling" by stimulating uPAR binding to matrix Vn. In support of this possibility we show that there is a strict correlation between the ability of pro-uPA to promote Vn binding and to induce ERK1/2-activation and changes in cell morphology (Fig. 3, Fig. 6, Fig. S2 B, and Fig. S4).

What is the molecular mechanism of uPAR-induced "Vn signaling"? The TIR-FM images and adhesion assays clearly demonstrate that expression of uPAR dramatically increases the contact between the cell and the ECM. Although uPAR does so passively by a physical interaction with matrix Vn, it will invariably bring all matrix receptors present in the plasma membrane in closer contact with their extracellular ligands. In the 293 cell line the uPAR-induced increase in cell/matrix contact triggers subsequent changes in cell morphology and signaling that are at least partially mediated by an RGD-dependent integrin, possibly $\alpha_v\beta_5$. Although it is possible that uPAR and integrins bind contemporarily to the same Vn molecule, this does not seem to be required because PAI-1, which is known to block integrin binding to Vn (Stefansson and Lawrence, 1996), induces similar changes when tethered to the cell membrane.

Because the Vn-binding form of uPAR is associated with membrane structures known as lipid rafts (Cunningham et al., 2003), the engagement of Vn by uPAR will bring these membrane domains in contact with the matrix. Lipid rafts are enriched in signal transduction molecules (Simons and Toomre, 2000) and the uPAR–Vn interaction will thus promote the tight encounter between the ECM, its different cell surface receptors, and the signal transduction machinery. As different cells have

different repertoires of membrane receptors and different matrices have different repertoires of ligands, our data suggest that the single interaction between uPAR and Vn may be responsible for many of the proteolysis-independent biological effects initiated by uPAR.

It is important to underscore that the conclusions of this work cannot be directly extrapolated to uPAR functions different from its ability to induce changes in cell morphology, basal cell migration, and ERK1/2 activation. For example, we have not assayed the ability of the different uPAR mutants to modulate directional cell migration and cell proliferation. Consequently, our data does not exclude nor confirm the requirement for additional direct uPAR interactions in these processes. Nevertheless, the identification of the Vn binding site presented here provides the first tool to directly address the importance of the Vn interaction in any experimental system where uPAR is expressed by transfection and/or infection. The single alanine substitution W32A efficiently disrupts the interaction with Vn while maintaining normal pro-uPA binding.

Materials and methods

Materials

CHO Flp-In and HEK293 Flp-In T-REx cells, expression vectors pcDNA5/FRT/TO and pOG44, zeocin, blasticidin S HCl, and Ham's F12 medium were from Invitrogen. Dulbecco's modified eagle medium (DME) and αMEM were from BioWhittaker. PBS, trypsin, glutamine, penicillin, and streptomycin were obtained from EuroClone, and fetal bovine serum (FBS) was from HyClone. Non-tissue culture plates were from Falcon Becton Dickinson. Tetracycline, poly-L-lysine, laminin (from Engelbreth-Holm-Swarm murine sarcoma), phalloidin-FITC, and CHO protein-free culture medium were from Sigma-Aldrich. FuGENE 6, fibronectin, and Hygromycin B were from Roche. Type-1 collagen from rat tail was from BD Biosciences. Urea-purified Vn was obtained from Promega. Pro-uPA was provided by Dr. Jack Henkin (Abbott Laboratories, Abbott Park, IL). Antibodies against total and phosphorylated ERK1/2 were from Cell Signaling Technology. Blocking antibodies against $\alpha_v\beta_3$ (LM609) and $\alpha_v\beta_5$ (P1F6) integrins were from Immunological Sciences. Monoclonal antibody against β_1 integrin (mAb 13) was from BD Biosciences. Monoclonal antibodies against human uPAR and the PAI-1 polyclonal antibody were provided by Dr. Gunilla Høyer-Hansen (Finsen Laboratory, Copenhagen, Denmark) and Dr. Peter Andreasen (Århus University, Århus, Denmark), respectively. Goat anti–mouse and goat anti–rabbit Ig F(ab')$_2$-FITC were from Jackson ImmunoResearch Laboratories.

Expression vector construction

The expression vector encoding full-length uPAR was generated by amplifying (oligos uPARu and uPARd) the human uPAR cDNA (Roldan et al., 1990) and cloned in the pcDNA5/FRT/TO vector using Kpn1/Not1. The expression vector encoding a GPI-anchored PAI-1 molecule was generated by uniting the complete PAI-1 coding region (aa −22 to 380), a short linker sequence (AlaGlyAlaGlyAlaGlyLys), and the GPI-anchoring signal sequence of uPAR (aa 276–313). The PAI-1 coding region and the linker region were generated by amplifying a HT1080 cDNA with oligos PAIu and PAId, and the GPI-anchor signal by amplifying the uPAR cDNA with oligos GPIu and uPARd. The PAI-1/linker fragment (Kpn1–HindIII) and the GPI fragment (HindIII–Not1) were assembled into Kpn1–Not1 digested pcDNA5/FRT/TO. The Vn(1–66)/Fc fusion protein was generated by attaching the first 66 amino acids of mature human Vn to a constant region of a human IgG. Primers and templates were as follows: a vector containing part of the Vn cDNA (pTrx-Vn(1–97) [Deng et al., 1996b]) amplified with oligonucleotides Vn(1–66)u and Vn(1–66)d and a vector containing an Fc region of human IgG (pIG-1 [Fawcett et al., 1992]) amplified with primers FcU and FcD. The Vn(1–66) (Kpn1–Xho1) and Fc (Xho1–Not) fragments were assembled in Kpn1–Not1 digested pcDNA5/FRT-TO. Variants of this construct where the SMB domain was deleted (Vn(40–66)/Fc) or where only the signal peptide was retained (Fc) were generated as above, substituting the oligo Vn(1–66)u with oligos Vn(40–66)u and SigU, respectively. The correct sequences of the complete coding regions of all constructs were verified by sequencing. All oligonuclotide sequences can be found in Table S1 (available at http://www.jcb.org/cgi/content/full/jcb.200612058/DC1). The expression vector encoding paxillin-GFP was provided by Dr. Alan F. Horwitz (University of Virginia, Charlottesville, VA; Laukaitis et al., 2001).

Site-directed mutagenesis

Alanine substitutions were generated by site-directed mutagenesis according to the QuikChange protocol (Stratagene). Alanine residues present in the uPAR sequence were substituted with glycine. Multiple rounds of mutagenesis were used to generate constructs carrying multiple substitutions. Expression vectors encoding soluble uPAR variants were generated by a second round of site-directed mutagenesis changing codon 284 of uPAR into a stop-codon (oligo pair A284Stop).

Cell culture

Parental HEK293 Flp-In T-REx cells were cultured in DME supplemented with 10% FBS, 100 U/ml penicillin, 100 U/ml streptomycin, 5 mM glutamine, 15 μg/ml blasticidin, and 100 μg/ml zeocin at 37°C in 5% CO_2. Parental CHO Flp-In cells were cultured in Ham's F12 supplemented as above, but without blasticidin. Transfections were performed with a 1:10 ratio of pcDNA5/FRT/TO-based expression vector and pOG44 using FuGENE 6, and stable HEK293 Flp-In T-Rex and CHO Flp-In transfectants were selected in medium lacking zeocin using 150 μg/ml and 300 μg/ml hygromycin B, respectively. Expression in HEK293 Flp-In T-REx was induced by adding 1 μg/ml tetracycline to the medium overnight.

Expression and purification of recombinant proteins

For the production of soluble uPAR mutants, semi-confluent CHO Flp-In stably transfected with the relevant expression vectors was washed with PBS and incubated for 7–10 d in CHO protein-free medium. The concentration of suPAR in the conditioned media was typically higher than 100 nM as determined by ELISA. The conditioned medium was used for in vitro binding assays without further purification. Recombinant Fc-fusion proteins were expressed in the same way, but were purified by standard Protein A affinity chromatography.

FACS analysis

Cell surface expression of integrins, uPAR, and PAI-1/GPI were analyzed by flow cytometry. $\alpha_v\beta_3$, $\alpha_v\beta_5$, and β_1-integrins were detected using primary antibodies (10 μg/ml). PAI-1/GPI was detected using a polyclonal antibody (2 μg/ml) and uPAR was detected using the monoclonal antibodies R2 and R4, as well as a polyclonal rabbit anti-uPAR antibody (all 2 μg/ml). Cells were stained with appropriate secondary FITC-labeled antibody (diluted 1:100) and analyzed by flow cytometry (FACSCalibur; BD Biosciences).

Scoring of cell morphology

For the scoring of cell morphology, changes induced by the different mutant receptors in semi-confluent cells were inspected by phase-contrast microscopy by three to five independent, trained observers. The observers were asked to score the morphology of the cells in comparison to uPAR and mock-transfected cells analyzed in parallel. A cumulative score of "uPAR" or "mock" morphology was assigned to clones where unanimous scoring by the individual observers was achieved. A cumulative score of "intermediate" morphology was assigned to clones where the majority (two or more) of the observers gave an "intermediate" score.

Adhesion assays

Adhesion assays were performed as described previously (Cunningham et al., 2003). In brief, cells were harvested, counted, and allowed to adhere in the presence or absence of 10 nM pro-uPA for 30 min at 37°C to 96-well plates (3×10^4 cells/well) coated with the different substrates as indicated. After washing, the adherent cells were fixed, stained with crystal violet, and quantified by measuring the absorbance at 540 nm. Coatings were as follows: 100 μg/ml poly-L-lysine, 10 μg/ml fibronectin, 10 μg/ml type-1 collagen, 20 μg/ml laminin, and 1 μg/ml vitronectin (Vn). Vn(1–66), Vn(1–66)^{RAD}, Vn(40–66), and Fc were all coated at 1 μg/ml.

Total internal reflection fluorescence microscopy (TIR-FM)

Cells were plated on glass coverslips and allowed to adhere overnight in the presence (293 cells) or absence (CHO cells) of 1 μg/ml tetracycline. Cells were washed in PBS, fixed in 4% paraformaldehyde, quenched with 30 mM NH_4Cl, permeabilized with 0.1% Triton X-100, 0.2% BSA in PBS,

and blocked with 2% BSA in PBS. Labeling of F-actin was performed using 0.2 μg/ml phalloidin-FITC, 1% BSA in PBS. TIR-FM imaging of cells was performed using a Biosystem TIR-FM workstation (Olympus) based on the Cell^R Imaging System (Olympus). A 488-nm argon laser was coupled in an inverted epifluorescence motorized microscope (IX81; Olympus) and focused at an off-axis position of the objective back focal plane. Cells plated on glass coverslips were viewed through a high-aperture 60× objective lens (UIS2 60× TIRFM PlanApo N, NA 1.45; Olympus) with an additional 1.6× lens. Images (16-bit depth) were acquired using an Orca-ER (C4742-80) Cooled CCD digital camera (Hamamatsu). Coverslips were directly inserted into an Attofluor Cell chamber (Invitrogen), rinsed with PBS (to maintain the requested difference of refractive indexes) and subjected to TIRF analysis. Time-lapse TIR-FM imaging was performed as above, with the exception that fixation/permeabilization/staining was omitted and that the cells were maintained at 37°C in normal growth medium throughout the recordings (every 15 s for a total of 15 min). Adjustment of brightness/contrast and smoothening of images was done using ImageJ 1.38i and always applied to the entire image.

Phase-contrast and time-lapse imaging

Phase-contrast and time-lapse live-cell imaging was performed at 37°C, 5% CO_2 with an inverted microscope (IX70; Olympus) equipped with an incubation chamber (Solent Scientific). Cells were always plated in serum-containing growth medium unless otherwise stated, and viewed through 20× (LCPlanFl, NA 0.4 Ph1, Olympus) or 40× (UIS2 40× UPlanFLN, NA 0.75 Ph2; Olympus) objective lenses with an additional 1.5× lens. All time-lapse acquisitions were performed using the 20× objective. The acquisition system includes a digital camera (Sensys; Roper Scientific) and System Control Software Metamorph 7.0r4 (Universal Imaging). Adjustment of brightness/contrast and smoothening of images was done using ImageJ 1.38i and always applied to the entire image. Cell migration speed was quantified with ImageJ 1.38i using the plug-in "manual tracking". In each experiment, 20 randomly chosen cells were tracked and their average migration speed throughout the experiment was calculated.

Binding assays of purified proteins

In vitro binding assays were performed essentially as described previously (Sidenius et al., 2002) using Nunc Maxisorb black-well plates for the detection of bound suPAR with an Eu^{3+}-labeled polyclonal anti-uPAR antibody (0.5 μg/ml) followed by the measurement of time-resolved fluorescence. Binding to immobilized Vn was measured using an excess of suPAR (80 nM) in the presence of a limiting concentration of pro-uPA (20 nM). All measurements were done in triplicate, and the specific binding calculated by subtraction of the nonspecific binding to BSA-coated wells.

Cell lysis and Western blotting

Cells were washed and lysed directly on the culture dish in ice-cold lysis buffer (25 mM Tris, pH 7.6, 150 mM NaCl, 1% Triton X-100, protease inhibitor cocktail [Complete-EDTA-free], 1 mM PMSF, 1 mM EDTA, 1 mM NaF, and 1 mM Na_3VO_4). After clarification by centrifugation (16,000 rcf, 15 min, 4°C) the total protein content was determined using the DC-Protein assay (Bio-Rad Laboratories) with BSA as standard. Equal amounts of total protein were separated by SDS-PAGE and probed as indicated.

Statistical analysis

The significance of differences in cell adhesion and ERK1/2 activation states were established using *t* test (paired, two-tailed) after log-transformation of the data from independent experiments.

Miscellaneous

The surface-accessible area of the residues of uPAR was calculated based on the A-chain of pdb-entry 1YWH (Llinas et al., 2005). Calculations were performed using the program AREAIMOL from the CCP4 suite of programs (Collaborative Computational Project, Number 4, 1994) with a probe-radius of 1.4 Å.

Online supplemental material

Fig. S1 (A and B) shows the profiling of Vn receptor expression and functionality in 293 cells. Fig. S1 (C and D) provides an example of comparable expression levels of the different mutants expressed in 293 cells. Fig. S2 A demonstrates that adhesion to Fn is unaffected by the expression of Vn-deficient uPAR mutants in 293 cells. Fig. S2 B and Fig. S4 show the rescue of morphological changes induced by exogenous pro-uPA for some uPAR mutants in 293 and CHO cells, respectively. Fig. S3 A indicates the migration speed of 293 cells expressing either Vn or integrin-deficient uPAR mutants. Fig. S3 B illustrates the crystal structure of the PAI-1–SMB complex and the position of the attached GPI anchor. Fig. S3 C illustrates the comparable cell surface expression level of uPAR and PAI-1. Table S1 lists information on all the mutants generated in this study, as well as all sequences of all oligonucleotides used in the study. Video 1 illustrates the increase in cell migration upon uPAR expression in 293 cells. Video 2 shows the redistribution of paxillin-GFP upon uPA-mediated rescue of uPAR/Vn binding in CHO cells. Video 3 shows the scattering effect upon uPA-mediated rescue of uPAR/Vn binding in preformed CHO colonies. Online supplemental material is available at http://www.jcb.org/cgi/content/full/jcb.200612058/DC1.

We thank Danika Trautmann for help with mutagenesis and Thomas R. Schneider for help with the evaluation of accessible surface areas. Massimiliano Garrè, Dario Parazzoli, and Mario Faretta from the Imaging Unit at IFOM are acknowledged for their assistance with microscopy. Dr. Francesco Blasi is acknowledged for helpful discussions.

This work was supported by grants from the European Union to Francesco Blasi (Integrated Project Cancerdegradome: CT 2003-503297 and Network of Excellence MAIN: CT 2003-502935) and from the Italian Association for Cancer Research (AIRC) and the Cariplo Foundation to N. Sidenius.

Submitted: 12 December 2006
Accepted: 3 May 2007

References

Aguirre Ghiso, J.A., K. Kovalski, and L. Ossowski. 1999. Tumor dormancy induced by downregulation of urokinase receptor in human carcinoma involves integrin and MAPK signaling. *J. Cell Biol.* 147:89–104.

Alfano, M., N. Sidenius, B. Panzeri, F. Blasi, and G. Poli. 2002. Urokinase-urokinase receptor interaction mediates an inhibitory signal for HIV-1 replication. *Proc. Natl. Acad. Sci. USA*. 99:8862–8867.

Barinka, C., G. Parry, J. Callahan, D.E. Shaw, A. Kuo, K. Bdeir, D.B. Cines, A. Mazar, and J. Lubkowski. 2006. Structural basis of interaction between urokinase-type plasminogen activator and its receptor. *J. Mol. Biol.* 363:482–495.

Blasi, F., and P. Carmeliet. 2002. uPAR: a versatile signalling orchestrator. *Nat. Rev. Mol. Cell Biol.* 3:932–943.

Chaurasia, P., J.A. Aguirre-Ghiso, O.D. Liang, H. Gardsvoll, M. Ploug, and L. Ossowski. 2006. A region in urokinase plasminogen receptor domain III controlling a functional association with alpha5beta1 integrin and tumor growth. *J. Biol. Chem.* 281:14852–14863.

Collaborative Computational Project, Number 4. 1994. The CCP4 suite: programs for protein crystallography. *Acta Crystallogr. D Biol. Crystallogr.* 50:760–763.

Cunningham, O., A. Andolfo, M.L. Santovito, L. Iuzzolino, F. Blasi, and N. Sidenius. 2003. Dimerization controls the lipid raft partitioning of uPAR/CD87 and regulates its biological functions. *EMBO J.* 22:5994–6003.

Degryse, B., M. Resnati, R.P. Czekay, D.J. Loskutoff, and F. Blasi. 2005. Domain 2 of the urokinase receptor contains an integrin-interacting epitope with intrinsic signaling activity: generation of a new integrin inhibitor. *J. Biol. Chem.* 280:24792–24803.

Deng, G., S.A. Curriden, S. Wang, S. Rosenberg, and D.J. Loskutoff. 1996a. Is plasminogen activator inhibitor-1 the molecular switch that governs urokinase receptor-mediated cell adhesion and release? *J. Cell Biol.* 134:1563–1571.

Deng, G., G. Royle, S. Wang, K. Crain, and D.J. Loskutoff. 1996b. Structural and functional analysis of the plasminogen activator inhibitor-1 binding motif in the somatomedin B domain of vitronectin. *J. Biol. Chem.* 271:12716–12723.

Fawcett, J., C.L. Holness, L.A. Needham, H. Turley, K.C. Gatter, D.Y. Mason, and D.L. Simmons. 1992. Molecular cloning of ICAM-3, a third ligand for LFA-1, constitutively expressed on resting leukocytes. *Nature.* 360:481–484.

Fazioli, F., M. Resnati, N. Sidenius, Y. Higashimoto, E. Appella, and F. Blasi. 1997. A urokinase-sensitive region of the human urokinase receptor is responsible for its chemotactic activity. *EMBO J.* 16:7279–7286.

Gardsvoll, H., B. Gilquin, M.H. Le Du, A. Menez, T.J. Jorgensen, and M. Ploug. 2006. Characterization of the functional epitope on the urokinase receptor. Complete alanine scanning mutagenesis supplemented by chemical cross-linking. *J. Biol. Chem.* 281:19260–19272.

Gargiulo, L., I. Longanesi-Cattani, K. Bifulco, P. Franco, R. Raiola, P. Campiglia, P. Grieco, G. Peluso, M.P. Stoppelli, and M.V. Carriero. 2005. Cross-talk between fMLP and vitronectin receptors triggered by urokinase receptor-derived SRSRY peptide. *J. Biol. Chem.* 280:25225–25232.

Gyetko, M.R., D. Aizenberg, and L. Mayo-Bond. 2004. Urokinase-deficient and urokinase receptor-deficient mice have impaired neutrophil antimicrobial activation in vitro. *J. Leukoc. Biol.* 76:648–656.

Høyer-Hansen, G., N. Behrendt, M. Ploug, K. Danø, and K.T. Preissner. 1997. The intact urokinase receptor is required for efficient vitronectin binding: receptor cleavage prevents ligand interaction. *FEBS Lett.* 420:79–85.

Huai, Q., A.P. Mazar, A. Kuo, G.C. Parry, D.E. Shaw, J. Callahan, Y. Li, C. Yuan, C. Bian, L. Chen, et al. 2006. Structure of human urokinase plasminogen activator in complex with its receptor. *Science.* 311:656–659.

Jensen, J.K., M.K. Durand, S. Skeldal, D.M. Dupont, J.S. Bodker, T. Wind, and P.A. Andreasen. 2004. Construction of a plasminogen activator inhibitor-1 variant without measurable affinity to vitronectin but otherwise normal. *FEBS Lett.* 556:175–179.

Jo, M., K.S. Thomas, D.M. O'Donnell, and S.L. Gonias. 2003. Epidermal growth factor receptor-dependent and -independent cell-signaling pathways originating from the urokinase receptor. *J. Biol. Chem.* 278:1642–1646.

Kjøller, L., and A. Hall. 2001. Rac mediates cytoskeletal rearrangements and increased cell motility induced by urokinase-type plasminogen activator receptor binding to vitronectin. *J. Cell Biol.* 152:1145–1157.

Laukaitis, C.M., D.J. Webb, K. Donais, and A.F. Horwitz. 2001. Differential dynamics of alpha 5 integrin, paxillin, and alpha-actinin during formation and disassembly of adhesions in migrating cells. *J. Cell Biol.* 153:1427–1440.

Li, Y., D.A. Lawrence, and L. Zhang. 2003. Sequences within domain II of the urokinase receptor critical for differential ligand recognition. *J. Biol. Chem.* 278:29925–29932.

Liang, O.D., K. Bdeir, R.L. Matz, T. Chavakis, and K.T. Preissner. 2003. Intermolecular contact regions in urokinase plasminogen activator receptor. *J. Biochem. (Tokyo).* 134:661–666.

Liu, D., J.A. Ghiso, Y. Estrada, and L. Ossowski. 2002. EGFR is a transducer of the urokinase receptor initiated signal that is required for in vivo growth of a human carcinoma. *Cancer Cell.* 1:445–457.

Llinas, P., M.H. Le Du, H. Gardsvoll, K. Dano, M. Ploug, B. Gilquin, E.A. Stura, and A. Menez. 2005. Crystal structure of the human urokinase plasminogen activator receptor bound to an antagonist peptide. *EMBO J.* 24:1655–1663.

Lund, L.R., K.A. Green, A.A. Stoop, M. Ploug, K. Almholt, J. Lilla, B.S. Nielsen, I.J. Christensen, C.S. Craik, Z. Werb, et al. 2006. Plasminogen activation independent of uPA and tPA maintains wound healing in gene-deficient mice. *EMBO J.* 25:2686–2697.

Mazzieri, R., S. D'Alessio, R.K. Kenmoe, L. Ossowski, and F. Blasi. 2006. An uncleavable uPAR mutant allows dissection of signaling pathways in uPA-dependent cell migration. *Mol. Biol. Cell.* 17:367–378.

Nguyen, D.H., I.M. Hussaini, and S.L. Gonias. 1998. Binding of urokinase-type plasminogen activator to its receptor in MCF-7 cells activates extracellular signal-regulated kinase 1 and 2 which is required for increased cellular motility. *J. Biol. Chem.* 273:8502–8507.

Nguyen, D.H., A.D. Catling, D.J. Webb, M. Sankovic, L.A. Walker, A.V. Somlyo, M.J. Weber, and S.L. Gonias. 1999. Myosin light chain kinase functions downstream of Ras/ERK to promote migration of urokinase-type plasminogen activator-stimulated cells in an integrin-selective manner. *J. Cell Biol.* 146:149–164.

Okumura, Y., Y. Kamikubo, S.A. Curriden, J. Wang, T. Kiwada, S. Futaki, K. Kitagawa, and D.J. Loskutoff. 2002. Kinetic analysis of the interaction between vitronectin and the urokinase receptor. *J. Biol. Chem.* 277:9395–9404.

Resnati, M., I. Pallavicini, J.M. Wang, J. Oppenheim, C.N. Serhan, M. Romano, and F. Blasi. 2002. The fibrinolytic receptor for urokinase activates the G protein-coupled chemotactic receptor FPRL1/LXA4R. *Proc. Natl. Acad. Sci. USA.* 99:1359–1364.

Roldan, A.L., M.V. Cubellis, M.T. Masucci, N. Behrendt, L.R. Lund, K. Danø, E. Appella, and F. Blasi. 1990. Cloning and expression of the receptor for human urokinase plasminogen activator, a central molecule in cell surface, plasmin dependent proteolysis. *EMBO J.* 9:467–474 (published erratum appears in *EMBO J.* 1990. May;9:1674).

Selleri, C., N. Montuori, P. Ricci, V. Visconte, M.V. Carriero, N. Sidenius, B. Serio, F. Blasi, B. Rotoli, G. Rossi, and P. Ragno. 2005. Involvement of the urokinase-type plasminogen activator receptor in hematopoietic stem cell mobilization. *Blood.* 105:2198–2205.

Sidenius, N., and F. Blasi. 2000. Domain 1 of the urokinase receptor (uPAR) is required for uPAR-mediated cell binding to vitronectin. *FEBS Lett.* 470:40–46.

Sidenius, N., and F. Blasi. 2003. The urokinase plasminogen activator system in cancer: recent advances and implications for prognosis and therapy. *Cancer Metastasis Rev.* 22:205–222.

Sidenius, N., A. Andolfo, R. Fesce, and F. Blasi. 2002. Urokinase regulates vitronectin binding by controlling urokinase receptor oligomerization. *J. Biol. Chem.* 277:27982–27990.

Simons, K., and D. Toomre. 2000. Lipid rafts and signal transduction. *Nat. Rev. Mol. Cell Biol.* 1:31–39.

Stefansson, S., and D.A. Lawrence. 1996. The serpin PAI-1 inhibits cell migration by blocking integrin alpha V beta 3 binding to vitronectin. *Nature.* 383:441–443.

Waltz, D.A., and H.A. Chapman. 1994. Reversible cellular adhesion to vitronectin linked to urokinase receptor occupancy. *J. Biol. Chem.* 269:14746–14750.

Wei, Y., D.A. Waltz, N. Rao, R.J. Drummond, S. Rosenberg, and H.A. Chapman. 1994. Identification of the urokinase receptor as an adhesion receptor for vitronectin. *J. Biol. Chem.* 269:32380–32388.

Wei, Y., M. Lukashev, D.I. Simon, S.C. Bodary, S. Rosenberg, M.V. Doyle, and H.A. Chapman. 1996. Regulation of integrin function by the urokinase receptor. *Science.* 273:1551–1555.

Wei, Y., X. Yang, Q. Liu, J.A. Wilkins, and H.A. Chapman. 1999. A role for caveolin and the urokinase receptor in integrin-mediated adhesion and signaling. *J. Cell Biol.* 144:1285–1294.

Wei, Y., J.A. Eble, Z. Wang, J.A. Kreidberg, and H.A. Chapman. 2001. Urokinase receptors promote beta1 integrin function through interactions with integrin alpha3beta1. *Mol. Biol. Cell.* 12:2975–2986.

Wei, Y., C.H. Tang, Y. Kim, L. Robillard, F. Zhang, M.C. Kugler, and H.A. Chapman. 2007. Urokinase receptors are required for alpha5beta1 integrin-mediated signaling in tumor cells. *J. Biol. Chem.* 282:3929–3939.